

Correlations Induced by Depressing Synapses in Quenched Critically Self-Organized Networks

João Guilherme Ferreira Campos,^{1,*} Ariadne de Andrade Costa,² Mauro Copelli,¹ and Osame Kinouchi³

¹*Departamento de Física, Universidade Federal de Pernambuco, 50670-901 Recife, PE, Brazil*

²*Instituto de Computação, Universidade Estadual de Campinas, 13083-852, Campinas, SP, Brazil*

³*Departamento de Física, FFCLRP, Universidade de São Paulo, 14040-901, Ribeirão Preto, SP, Brazil*

In a recent work, mean-field analysis and computer simulations were employed to analyze critical self-organization in annealed networks of excitable cellular automata, where randomly chosen links were depressed after each spike. Calculations agree with simulations of the annealed version, showing that the nominal *branching ratio* σ converges to unity in the thermodynamic limit, as expected of a self-organized critical system. However, the question remains whether the same results apply to a biologically more plausible, quenched version, in which the neighborhoods are fixed, and only the active synapses are depressed. We show that simulations of the quenched model yield significant deviations from $\sigma = 1$, due to spatial correlations. However, the model is shown to be critical, as the largest eigenvalue λ of the synaptic matrix is shown to approach unity in the thermodynamic limit. We also study the finite size effects near the critical state as a function of the parameters of the synaptic dynamics.

PACS numbers: 05.65.+b, 05.70.Ln, 07.05.Mh

I. INTRODUCTION

The first empirical evidence of criticality in the brain was given by Beggs and Plenz, who reported that in vitro rat cortex slices exhibit neuronal avalanches with power law distribution with exponents $-3/2$ and -2 for avalanche size and duration, respectively [1]. This was regarded as evidence that the brain as a dynamical system fluctuates around a critical point, presumably similar to a critical branching process with the branching parameter close to unity. Either on theoretical or experimental grounds, this property has been shown to optimize computational capabilities [2], information transmission [1, 3], and sensitivity to stimuli [4–7], among others, as recently reviewed in Refs. [8, 9].

In order to explain the self-organization around the critical point, Arcangelis *et al.* [10] introduced a model with synaptic depression and synaptic recovery (see also [11, 12]). They obtained Self-Organized Criticality (SOC) and other very interesting results but their synaptic depression mechanism has the undesirable feature of depending on non-local information. In contrast, Levina, Herrmann and Geisel (LHG) proposed a local model which consists of a fully connected network of integrate and fire neurons, such that when a neuron fires, the strength of its output links (synapses) are reduced by a fraction [13]. This fast dissipation mechanism is associated with short-term synaptic depression due to temporary neurotransmitter vesicle depletion. It is countered by a loading mechanism at a different time scale, by which synaptic neurotransmitters are slowly replenished when the synapse is idle. LHG claimed their model exhibit SOC, based on the emergence of power-law dis-

tributions of avalanche sizes.

On a pair of review papers, however, Bonachela *et al.* showed that for a system to exhibit SOC its bulk dynamics must be conservative at least in average [14–16]. They showed that systems with dissipative and loading mechanisms such as the LHG model would hover around the critical point with nonvanishing fluctuations even in the thermodynamic limit. In that sense, the behavior of the LHG model would not be classified as SOC, but rather was called Self Organized quasi-Criticality (SOqC). Indeed, the LHG model seems to pertain to the Dynamical Percolation class [15] and not to the Directed Percolation class as is usual in *bona fide* SOC models.

In a recent work, we analyzed a random neighbor network of excitable cellular automata with dynamical synapses [17]. It was inspired by the LHG model, but with three different ingredients: finite connectivity (with K outgoing synapses in a random graph), discrete state units and multiplicative probabilistic synapses. In its annealed version, K randomly chosen synapses are depressed whenever any neuron spikes. The model was shown to behave differently from the LHG model, in that not only did the nominal branching ratio σ converged to unity but, perhaps most importantly, the fluctuations around the criticality condition $\sigma = 1$ vanished in the thermodynamic limit. Also, the associated phase transition is standard: continuous, with one absorbing state, and in the Directed Percolation universality class.

Despite the agreement between the mean-field calculations and the numerical simulations, a major drawback of the annealed model is its lack of biological plausibility. Here we investigate in detail the quenched version of the model, in which, when a presynaptic neuron fires, its outgoing synapses are depressed. In particular, we focus on whether the quenched model behaves similarly to the annealed model as far as SOC is concerned.

The rest of the paper is structured as follows. In sec-

* joaogfc@gmail.com

tion 2, we revisit the model, and in particular the differences between annealed and quenched networks. In section 3, we present our simulation results and discussions. Concluding remarks appear in section 4.

II. THE MODEL

Our model builds upon a random-neighbor network of excitable automata neurons (quiescent ($S_j = 0$), to firing ($S_j = 1$), to refractory ($S_j = 2, 3, \dots, n-1$), to quiescent ($S_j = 0, j = 1, \dots, N$)) used previously [4, 17]. In this version, N sites with states $S_j(t)$ have each exactly $K_j^{out} = K$ outlinks to postsynaptic neurons $S_i(t)$ coupled via probabilistic synapses $P_{ij}(t)$, which define a connectivity matrix. With this construction, each neuron has K_j^{in} binomially distributed incoming links with average K . After a site spikes, it deterministically becomes refractory for $n-2$ time steps [$S_j(t+2) = 2, S_j(t+3) = 3, \dots, S_j(t+n-1) = n-1$] and then returns to quiescence (for details, see Ref. [17]). On the quenched case, the synapses are dynamic and their evolution obeys the following equation:

$$P_{ij}(t+1) = P_{ij}(t) + \frac{\epsilon}{KN^a} (A - P_{ij}(t)) - uP_{ij}(t)\delta(t-t_j), \quad (1)$$

where ϵ is the coefficient of synaptic recovery, A is the asymptotic synaptic value and u is the fraction of synaptic coupling that is lost whenever a neuron fires. The $\{t_j\}$ are the time intervals when the neuron j fires, which means that, whenever a neuron fires, all its outgoing synapses are reduced to $(1-u)$ of their original value. The exponent a enable us to explore how the model behaves with different scalings with N for the synaptic recovery dynamics.

On the other hand, for annealed networks, instead of depressing the K outgoing synapses of a given neuron, either K randomly chosen synapses are depressed after a given spike or a random neuron is chosen and its K outgoing synapses are depressed after a given spike. The purpose of the annealed case is to destroy correlations between the P_{ij} , so one can use mean-field analysis to get a better insight of the problem, as done previously [17]. Both annealed cases work equally well in destroying correlations, but the latter is computationally more efficient.

The initial conditions for the synapses are defined by choosing σ_0 and uniformly drawing random values to $P_{ij}(0)$ in the interval $[0, 2\sigma_0/K]$. The system is set in the slow driving limit. The initial condition is $S_i(0) = 0$ for all $i \neq k$ and $S_k(0) = 1$, i. e., we start an avalanche at site k . Whenever the system returns to quiescence (that is, the absorbing state $S_i(t) = 0, \forall i$), we start another avalanche by choosing a random neuron l , and setting $S_l(t+1) = 1$.

We let the system evolve and after a transient period it approaches a stationary state. At each time step we compute a local branching ratio $\sigma_j(t) = \sum_{i=1}^K P_{ij}(t)$ and

a global branching ratio $\sigma(t) = \frac{1}{N} \sum_{j=1}^N \sigma_j(t)$. In the stationary state, $\sigma(t)$ oscillates around some average value σ^* with standard deviation $\Delta\sigma^*$. As shown in [17], the mean-field analysis predicts that:

$$\sigma^* \simeq 1 + \frac{(AK-1)}{1+x}, \quad (2)$$

where $x \equiv uKN^a/[(n-1)\epsilon]$. This result only holds for $A > 1/K$ (notice that perfect criticality can be achieved with the choice $A = 1/K$ but this is a fine tuning for the A parameter that should not be used in the SOC context). In the limit $x \gg 1$, we get:

$$\sigma^* \simeq 1 + \frac{\Omega}{N^a}, \quad (3)$$

where $\Omega \equiv (AK-1)(n-1)\epsilon/(uK)$. That is, the mean-field analysis predicts that, for $a > 0$ and large N , σ^* differs from $\sigma_c = 1$ by a factor of order $1/N^a$, therefore $\sigma^* \rightarrow 1$ in the infinite-size limit. The case $a = 0$ will be discussed separately.

We define the Perron-Froebenius (largest) eigenvalue of the connectivity matrix $P_{ij}(t)$ as $\lambda(t)$, which in the stationary state oscillates around the mean value λ^* with standard deviation $\Delta\lambda^*$. As shown previously by Larremore *et al.* [18], the phase transition between an absorbing and an active phases occurs at $\lambda_c = 1$. The question then arises: does the quenched model converges to λ_c and, if so, how do the fluctuations behave?

In the next section, we analyze the behavior of λ^* and σ^* , and their respective standard deviations, with our model parameters ϵ, u, A, K , as a function of N . We concentrate on the case $a = 1$ since all previous literature examined this scaling [13, 15, 17], but we also discuss briefly other values for the exponent a .

III. SIMULATION RESULTS

To simplify our simulations we fix $K = 10$, meaning that the number of outgoing synapses is much smaller than the number of neurons. If we fix ϵ and plot σ^* and λ^* while we vary N (with exponent $a = 1$), we obtain Fig. 1. Observe in Fig. 1a that, for annealed networks, when ϵ is small, σ^* is smaller than 1 and is independent of N ; but as ϵ increases, σ^* also increases until it starts behaving like Eq. 3 for $\epsilon \gtrsim 8$. For these values of ϵ , we also plot in Fig. 1a the curves predicted by Eq. 2.

For quenched networks, the behavior is quite similar, as shown in Fig. 1c. However, as we increase ϵ , σ^* behaves as:

$$\sigma^* \simeq 1.105 + \frac{\Omega_q}{N}, \quad (4)$$

for some constant Ω_q , instead of following Eq. 3. That indicates that mean-field theory does not describe well the quenched case. Furthermore, if we fix N and vary

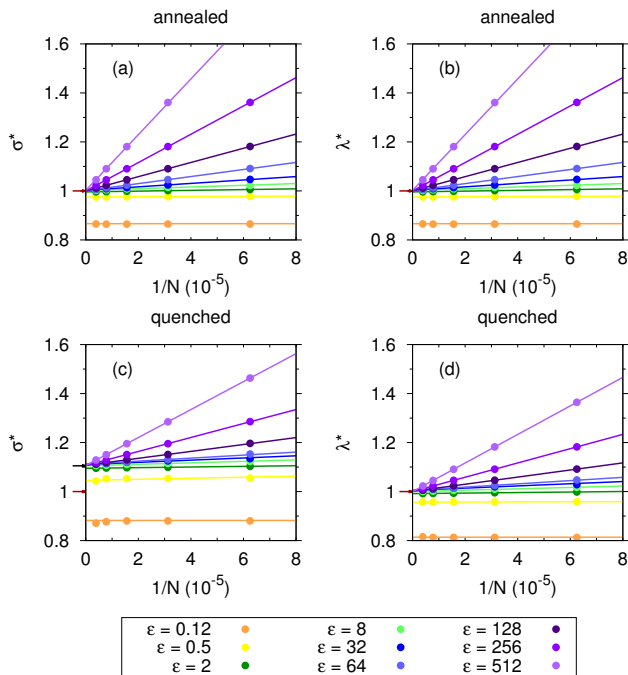


FIG. 1. σ^* and λ^* versus $1/N$ for several values of ϵ for quenched and annealed networks. The error bars do not appear in this scale. The lines are curves of the type $f(N) = \alpha + \beta/N$ that best fit the data, except for (a) where the curves are the given by Eq. 3 for $\epsilon \geq 8$. Parameters: $n = 3$, $K = 10$, $A = 1.0$, $u = 0.1$, $a = 1$.

ϵ , as in Fig. 2, we see that for annealed networks (Fig. 2a) $\sigma^* \approx 1$ for a wide range of the parameter values that gets bigger as N increases. However for quenched networks (Fig. 2c) we see the same behavior with $\sigma^* \approx 1.105$ instead of 1. The same apparently strange behavior of quenched networks does not appear in the plots for λ^* shown in Fig. 1d and 2d. This occurs because σ^* is the wrong “control” parameter: λ^* is the correct predictor for criticality, as shown by Larremore *et al.* [18].

If we plot λ^* versus σ^* for all the simulations shown in Figs. 1 and 2 we get Fig. 3a. Notice that for quenched networks we obtain $\sigma^* = 1.105$ exactly when $\lambda^* = 1$ (Fig. 3a), meaning that λ^* indeed approaches a critical value in quenched networks (see Fig. 1 and 2). Moreover, in the annealed networks the points lie exactly in the identity curve (Fig. 3a). This is consistent with the known result that the equality $\sigma = \lambda$ holds only when there are no correlations between the P_{ij} [18].

The question still remains of what are these correlations and how do they arise. Similarly to the local branching ratio $\sigma_i(t)$, we can define the local converging ratio $\sigma_i^{in}(t) = \sum_j P_{ij}(t)$. According to Ref. [19], $\lambda_t = \langle \sigma(t)\sigma^{in}(t) \rangle / \sigma_t$, where for a given observable O , $\langle O \rangle = \frac{1}{N} \sum_i O_i$. In Fig. 3b, we plot $\sigma_i(t)$ versus $\sigma_i^{in}(t)$ in the stationary regime for annealed networks. Notice that the two quantities seem to be uncorrelated (Spearman correlation coefficient -0.002), giving $\lambda_t = \sigma_t$, where

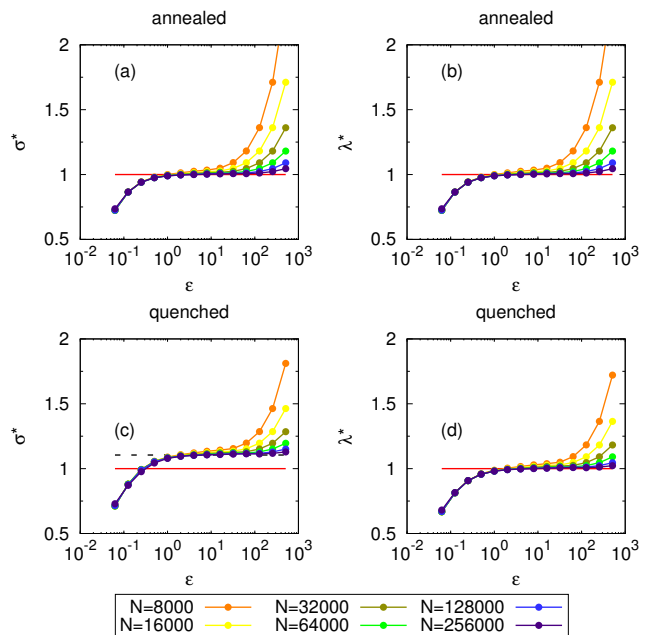


FIG. 2. σ^* and λ^* versus ϵ for several values of N for quenched and annealed networks. The error bars do not appear in this scale. The red line is the critical value 1 and the dashed line is 1.105. The other lines are guides to the eye. Parameters: $n = 3$, $K = 10$, $A = 1.0$, $u = 0.1$, $a = 1$.

we used that $\langle \sigma_i(t) \rangle = \langle \sigma_i^{in}(t) \rangle = \sigma_t$. In Fig. 3c we show the same result for quenched networks. Now the two quantities are negatively correlated (Spearman coefficient -0.696) and, consistently, $\lambda_t \neq \sigma_t$. The negative correlation has an intuitive explanation: if a given site has a high (low) local converging ratio, it will spike more (less) often, depressing more (less) its synapses, which implies a lower (higher) probability of exciting its neighbors.

In Fig. 1 we see that all curves are straight lines. Thus, aiming at understanding the behavior of the networks as $N \rightarrow \infty$, we fit the data with curves of the type $f_\sigma(N) = \alpha_\sigma + \frac{\beta_\sigma}{N}$ and $f_\lambda(N) = \alpha_\lambda + \frac{\beta_\lambda}{N}$ for σ^* and λ^* , respectively, as shown in Fig. 1 (except for σ^* for $\epsilon \geq 8$ in the annealed case, where we show the theoretical curve). We also observe that $\lim_{N \rightarrow \infty} \sigma^* = \alpha_\sigma$ and $\lim_{N \rightarrow \infty} \lambda^* = \alpha_\lambda$ and plot them as a function of ϵ . The result is shown in Fig. 4.

For annealed networks and $\epsilon \gtrsim 4$, we obtain $\lim_{N \rightarrow \infty} \sigma^* = 1$, within errors (Fig. 4a). For quenched networks and $\epsilon \gtrsim 8$, we obtain $\lim_{N \rightarrow \infty} \sigma^* = 1.105$, within errors (Fig. 4c). On the other hand, $\lim_{N \rightarrow \infty} \lambda^* = 1$, within errors, for $\epsilon \gtrsim 4$ (annealed, Fig. 4b) and $\epsilon \gtrsim 8$ (quenched, Fig. 4d). That is, quenched (annealed) networks are either subcritical, if $\epsilon \lesssim 8$ ($\epsilon \lesssim 4$), or critical, if $\epsilon \gtrsim 8$ ($\epsilon \gtrsim 4$), in the infinite size limit, but never supercritical. This means that there is a semi-infinite volume in the (ϵ, A, u) parameter space with critical α_λ . This is one of the most important results of the paper.

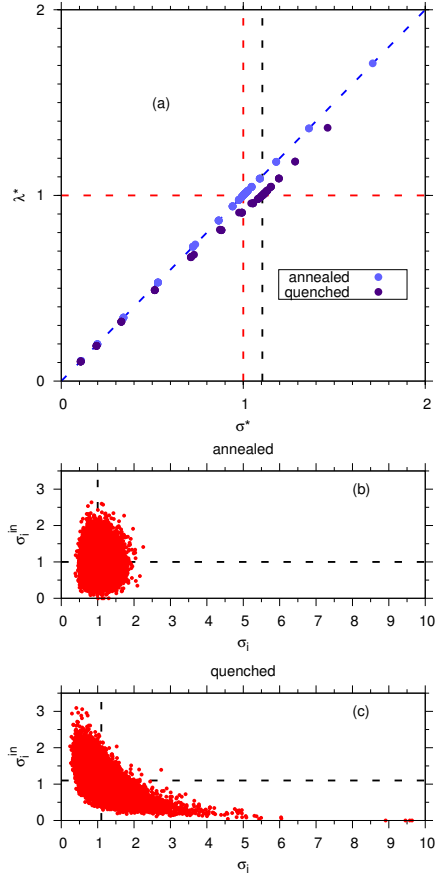


FIG. 3. (a) λ^* versus σ^* for several values of N and ϵ for quenched and annealed networks. The red dashed lines are $\lambda^*, \sigma^* = 1$, the blue dashed line is the identity function $\lambda^* = \sigma^*$ and the black dashed line is $\sigma^* = 1.105$. Other parameters: $n = 3, K = 10, A = 1.0, u = 0.1, a = 1$. (b) and (c) σ_i^{in} versus σ_i for annealed and quenched networks, respectively, with $N = 32000$ and $\epsilon = 2$. The dashed lines are the curves $\sigma_i, \sigma_i^{in} = 1.0$ in the annealed case and $\sigma_i, \sigma_i^{in} = 1.105$ in the quenched case. Other parameters are the same as before. The Spearman correlation coefficient for the annealed network (b) is -0.002 (no correlation), and for the quenched network (c) is -0.696 (strong negative correlation).

Since $\lambda \simeq \sigma$ for annealed networks, and since the behavior of λ is qualitatively the same for both annealed and quenched networks, from now on we focus on quenched networks only. In the following, we present the study of the influence of parameter A on the values of σ^* and λ^* , for different network sizes (Fig. 5a,b). The system becomes subcritical only for small values of A . It occurs because in the synaptic dynamic we have $(A - P_{ij})$, which implies that $P_{ij} \rightarrow A$ in the limit of no activity. Since we need $P_{ij} = 1/K$ to achieve critical avalanches, A must satisfy $A > 1/K = 0.1$. Lower values of A take the network to subcritical states regardless of ϵ and u . Nevertheless, for $A > 1/K$, the system becomes critical as the size is increased.

In Fig. 5c,d we exhibit the variation of σ^* and λ^* , re-

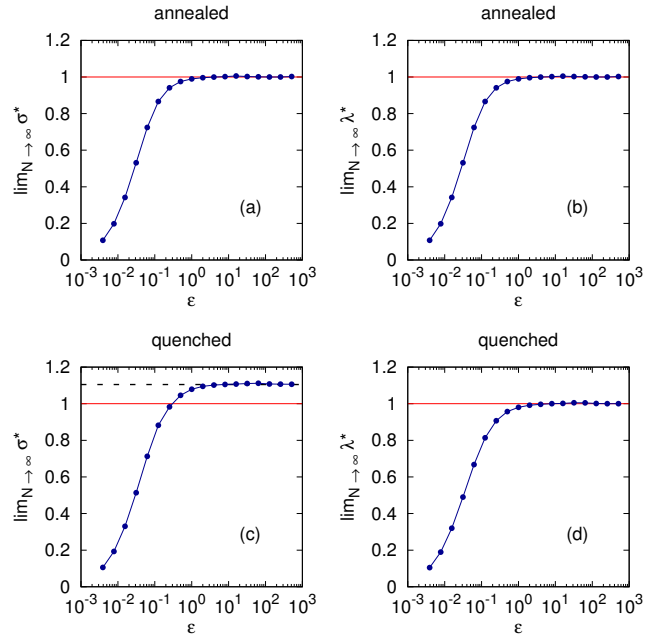


FIG. 4. The limit of σ^* and λ^* when N goes to infinity versus the parameter ϵ for quenched and annealed networks. The red line is the critical value 1 and the dashed line is 1.105. The blue line is a guide to the eye. Parameters: $n = 3, K = 10, A = 1.0, u = 0.1$ and $a = 1$.

spectively, as a function of u . We can see that σ^*, λ^* decreases with u , as expected. It is notable that λ^* converges to 1 for every u as the system size is increased.

Interesting results are also obtained by studying the dependence on the number K of neighbors. Figure 5e reveals that σ^* decreases with K , whereas Fig. 5f shows that λ^* stays approximately constant. For increasing K , the systems approaches a complete graph for which annealed and quenched cases are equal. This means that correlations in the system decrease with increasing K and σ^* approaches λ^* . Again λ^* converges to 1 as the system size is increased.

Now we understand that $\lambda^* \rightarrow 1$ when $N \rightarrow \infty$ for a wide range of the parameter space of the model. Hence, we focus on the behavior of λ_t . In Fig. 6 we plot λ_t versus t , starting from different initial conditions for λ_0 . We see that irrespective of the initial conditions, the network self-organizes towards the critical value $\lambda^* \approx \lambda_c = 1$.

In Fig. 7 we present histograms for λ_t for different values of ϵ and N . The data is collected every 100 time steps during a time span of 10^6 time steps, after a transient. We see that the width of the histograms decreases as N grows. So we have a SOC behavior, similar to conservative models with static parameters. However, for $\epsilon = 64$ this is not so apparent because N is not sufficiently large (Fig. 7d). This reveals that, although the model is very robust, for small networks the system is considerably dependent on the parameter space. In particular, the average λ moves from supercritical values for

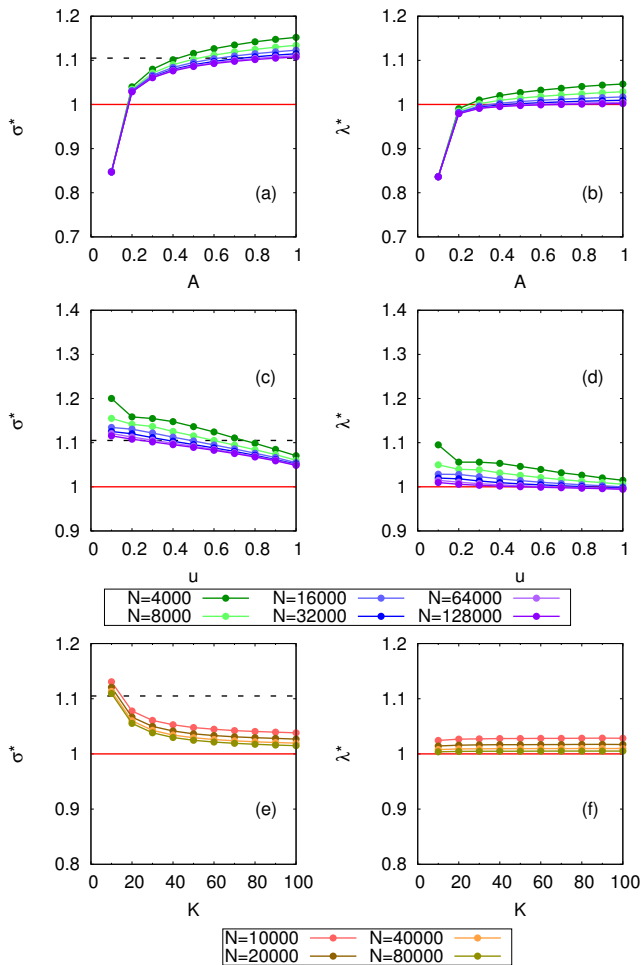


FIG. 5. (a) and (b) σ^* and λ^* , respectively, versus A as N increases. Parameters: $\epsilon = 8$, $n = 3$, $K = 10$, $u = 0.1$, $a = 1$. (c) and (d) σ^* and λ^* , respectively, versus u as N increases. Parameters: $\epsilon = 32$, $n = 3$, $K = 10$, $A = 1.0$, $a = 1$. (e) and (f) σ^* and λ^* , respectively, versus K as N increases. Parameters: $\epsilon = 8$, $n = 3$, $A = 1.0$, $u = 0.1$, $a = 1$. The error bars do not appear in the scales. The red line is the critical value 1 and the dashed line is 1.105. The figure comes from quenched networks.

small N toward the critical value for large N .

Bonachela *et al.* [15] found a similar finite size behavior in the LHG model. They also found, both from a field theory and from simulations, that there exists a better scaling with N which puts the network always at criticality, with good power laws, for any N . This occurs if we use a N^a scaling with exponent $a = 2/3$, or equivalently, if we use $a = 1$ with $\epsilon \propto N^{1/3}$.

To check this, we present similar histograms for λ_t (Fig. 8), but now using the scaling $\epsilon = 0.07N^{1/3}$. We see that with this scaling we obtain well behaved networks that are always critical, that is, have the average λ_t equal to 1 for all N . This peculiar exponent $1/3$ also appears in other models [14, 20], with similar results. In Fig. 8, we see that $P(\lambda_t)$ sharpens as N is increased.

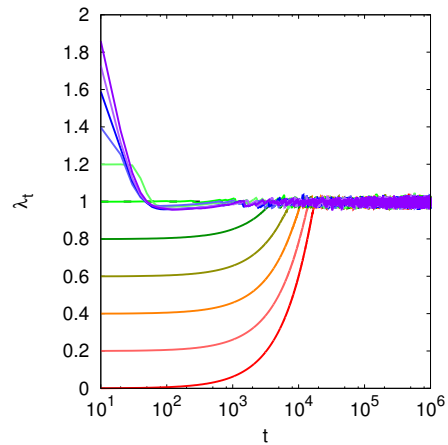


FIG. 6. Evolution of λ_t versus t for several different initial values. All curves reach a stationary mean value $\lambda^* \simeq 1$ after a transient time. Parameters: $N = 32000$, $\epsilon = 2$, $n = 3$, $K = 10$, $A = 1.0$, $u = 0.1$ and $a = 1$.

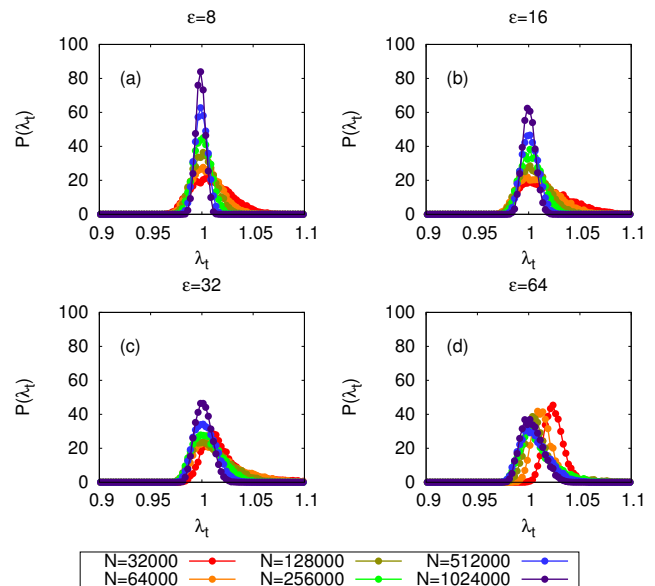


FIG. 7. Histograms of λ_t for quenched networks with fixed $\epsilon = 8, 16, 32$ and 64 . The lines are guides to the eye. Parameters: $n = 3$, $K = 10$, $A = 1.0$, $u = 0.1$ and $a = 1$.

Therefore, we conclude that, for $a > 0$, the fluctuations of $\lambda(t)$ around the mean value decrease for increasing system size and presumably vanish in the infinite-size limit. This result strongly differs from that is found for the LHG model [15], where fluctuations do not vanish for large N . Indeed, due to this fact, Bonachela *et al.* proposed that the LHG model pertains to the Dynamical Percolation universality class, not the Directed Percolation class as standard SOC models. Our model, in contrast, clearly pertains to the Directed Percolation class, but is not clear what is the decisive difference be-

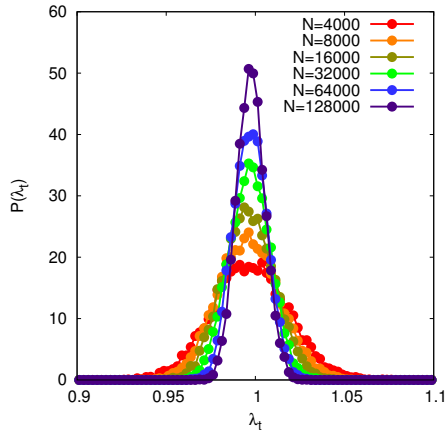


FIG. 8. Histograms of λ_t for quenched networks with $\epsilon = 0.07N^{1/3}$. The lines are guides to the eye. Parameters: $n = 3$, $K = 10$, $A = 1.0$, $u = 0.1$.

tween ours and the LHG model that produces this change of universality class. In fact, it would be interesting to extend this analysis to other analytically treatable models in which signs of criticality have been found, such as the non-conservative neuronal networks exhibiting up and down states proposed by Millman et al. [21]. This is an open problem to be addressed in the future.

Finally, let us discuss the case $a = 0$, which means that the synaptic recovery dynamics does not depend on N . Indeed, this is the biologically realistic case since the recovery time can not depend on non-local information like the network size N . Our mean-field result predicts:

$$\sigma^* \simeq 1 + \frac{(AK - 1)}{1 + x}, \quad (5)$$

where now $x \equiv uK/[(n - 1)\epsilon]$. Since x is always finite, the stationary value σ^* is always supercritical (and the same we expect for λ^*). However, by using $AK \geq 1$, say $A = 1.1/K$, and a biologically motivated value for the number of synapses ($K = 10^4$), we get with the values $n = 3$, $u = 1$, $\epsilon = 4$:

$$\sigma^* \simeq 1.0088, \quad (6)$$

which, although supercritical, seems to be sufficiently close to criticality to explain the experimental power laws in neuronal avalanches. Notice that this mean-field result is also relevant to the quenched case since, as can be seen in Fig. 5e, we have $\sigma^* \rightarrow \lambda_c = 1$ for large K . This slightly supercriticality has been called *self-organized supercriticality* (SOSC) by Brochini *et al.* [22]. Curiously, superavalanches (the so called *dragon kings*) and supercriticality have also been observed in experiments [11].

IV. CONCLUSION

The nominal branching ratio σ is a good predictor of criticality only for annealed networks, whose definition is

such that correlations are destroyed by construction. If σ is used to assess criticality in quenched networks, it incorrectly predicts supercriticality. The largest eigenvalue λ of the synaptic matrix, on the other hand, is a better predictor of criticality than σ , in that it is robust against correlations. We stress that such correlations do not arise from the network topology as in Ref. [18] (Erdős-Rényi random networks with quenched synapses present $\sigma_c = \lambda_c = 1$ instead of $\sigma_c > \lambda_c$, see [4]), but from the dynamics in the links.

When the proposed mechanism of synaptic depression, Eq. (1), is tested with λ instead of σ , it consistently points to a convergence to a self-organized critical regime, for annealed as well as for quenched networks, if we use a recovery time scaling with N^a and $a > 0$.

Intensive numerical simulations have been employed and the data have been carefully analyzed leading us to the conclusion that if the synapses recover fast enough (large enough ϵ), quenched networks are critical in the infinite-size limit. Besides that, as this limit is approached, the fluctuations around the mean value become increasingly small, which means that large enough networks will be indistinguishable from critical ones (and we must remember that biological networks are very large, $N > 10^6$). So, the mean-field calculation and the simulations both suggest that there is a semi-infinite volume in the parameter space (ϵ, A, u) that produces SOC behavior in the infinite size limit.

Finally, the case with $a = 0$ only produces Self-Organized Supercriticality (SOSC [22]). However, for large number of synapses K , as suggested by biology, networks which are almost critical are obtained, and this can be sufficient to deal with the power laws found in experiments.

Moreover, the SOSC scenario suggests that biological neuronal networks could be indeed slightly supercritical, a fact perhaps masked by standard experiments with few electrodes but sometimes revealed in dragon kings avalanches [11]. This SOSC scenario (exponent $a = 0$ case) should be studied more deeply in another publication.

ACKNOWLEDGMENTS

This article was produced as part of the activities of FAPESP Research, Innovation and Dissemination Center for Neuromathematics (grant #2013/07699-0, S.Paulo Research Foundation). We acknowledge financial support from CAPES, CNPq, FACEPE, and CNAIPS-USP. AAC thanks FAPESP (grant #2016/00430-3).

-
- [1] J. M. Beggs and D. Plenz, *J. Neurosci.* **23**, 11167 (2003).
- [2] N. Bertschinger and T. Natschläger, *Neural Comput.* **16**, 1413 (2004).
- [3] W. L. Shew, H. Yang, S. Yu, R. Roy, and D. Plenz, *J. Neurosci.* **31**, 55 (2011).
- [4] O. Kinouchi and M. Copelli, *Nat. Phys.* **2**, 348 (2006).
- [5] W. Shew, H. Yang, T. Petermann, R. Roy, and D. Plenz, *J. Neurosci.* **29**, 15595 (2009).
- [6] S. H. Gautam, T. T. Hoang, K. McClanahan, S. K. Grady, and W. L. Shew, *PLoS Comput Biol* **11**, 1 (2015).
- [7] M. Girardi-Schappo, G. S. Bortolotto, J. J. Gonsalves, L. T. Pinto, and M. H. R. Tragtenberg, *Sci. Rep.* **6** (2016).
- [8] D. R. Chialvo, *Nat. Phys.* **6**, 744 (2010).
- [9] W. Shew and D. Plenz, *Neuroscientist* **19**, 88 (2013).
- [10] L. de Arcangelis, C. Perrone-Capano, and H. J. Herrmann, *Phys. Rev. Lett.* **96**, 028107 (2006).
- [11] L. de Arcangelis, *Eur. Phys. J. Spec. Top.* **205**, 243 (2012).
- [12] F. Lombardi, H. J. Herrmann, D. Plenz, and L. de Arcangelis, *Sci. Rep.* **6**, 24690 (2016).
- [13] A. Levina, J. M. Herrmann, and T. Geisel, *Nat. Phys.* **3**, 857 (2007).
- [14] J. A. Bonachela and M. A. Muñoz, *J. Stat. Mech.* **2009**, P09009 (2009).
- [15] J. A. Bonachela, S. de Franciscis, J. J. Torres, and M. A. Muñoz, *J. Stat. Mech.* **2010**, P02015 (2010).
- [16] S. A. Moosavi and A. Montakhab, *Phys. Rev. E* **89**, 052139 (2014).
- [17] A. A. Costa, M. Copelli, and O. Kinouchi, *J. Stat. Mech.* **2015**, P06004 (2015).
- [18] D. B. Larremore, W. L. Shew, and J. G. Restrepo, *Phys. Rev. Lett.* **106**, 058101 (2011).
- [19] J. G. Restrepo, E. Ott, and B. R. Hunt, *Phys. Rev. E* **76**, 056119 (2007).
- [20] G. Pruessner and H. J. Jensen, *EPL (Europhysics Letters)* **58**, 250 (2002).
- [21] D. Millman, S. Mihalas, A. Kirkwood, and E. Niebur, *Nat. Phys.* **6**, 801 (2010).
- [22] L. Brochini, A. A. Costa, M. Abadi, A. C. Roque, J. Stolfi, and O. Kinouchi, *arXiv preprint arXiv:1606.06391* (2016).